Viscoelastic properties of plasma-agarose hydrogels dictate favorable fibroblast responses for skin tissue engineering applications

Patiño Vargas, Maria Isabel; Martinez-Garcia, Francisco Drusso; Offens, Freya; Becerra, Natalia Y.; Restrepo, Luz M.; van der Mei, Henny C.; Harmsen, Martin C.; van Kooten, Theo G.; Sharma, Prashant K.

Published in:
Biomaterials Advances

DOI:
10.1016/j.bioadv.2022.212967

Publication date:
2022

139 (2022) 212967

Contents lists available at ScienceDirect

Biomaterials Advances

journal homepage: www.journals.elsevier.com/materials-science-and-engineering-c

Viscoelastic properties of plasma-agarose hydrogels dictate favorable fibroblast responses for skin tissue engineering applications

Maria Isabel Patiño Vargas [a,b,1], Francisco Drusso Martinez-Garcia [c,1], Freya Offens [a], Natalia Y. Becerra [b], Luz M. Restrepo [b], Henny C. van der Mei [a], Martin C. Harmsen [c], Theo G. van Kooten [a], Prashant K. Sharma [a,*]

[a] University of Groningen, University Medical Center Groningen, Department of Biomedical Engineering, Groningen, the Netherlands
[b] Tissue Engineering and Cell Therapy Group, Faculty of Medicine, University of Antioquia, Medellín, Colombia
[c] University of Groningen, University Medical Center Groningen, Department of Pathology and Medical Biology, Groningen, the Netherlands

ARTICLE INFO

Keywords:
Plasma
Agarose
Hydrogel
Viscoelasticity
Fibroblasts
Maxwell model

ABSTRACT

Dermal wound healing relies on the properties of the extracellular matrix (ECM). Thus, hydrogels that replicate skin ECM have reached clinical application. After a dermal injury, a transient, biodegradable fibrin clot is instrumental in wound healing. Human plasma, and its main constituent, fibrin would make a suitable biomaterial for improving wound healing and processed as hydrogels albeit with limited mechanical strength. To overcome this, plasma-agarose (PA) composite hydrogels have been developed and used to prepare diverse bioengineered tissues. To date, little is known about the influence of variable agarose concentrations on the viscoelastic properties of PA hydrogels and their correlation to cell biology. This study reports the characterization of the viscoelastic properties of different concentrations of agarose in PA hydrogels: 0 %, 0.5 %, 1 %, 1.5 %, and 2 % (*w/v*), and their influence on the cell number and mitochondrial activity of human dermal fibroblasts. Results show that agarose addition increased the stiffness, relaxation time constants 1 (τ1) and 2 (τ2), and fiber diameter, whereas the porosity decreased. Changes in cell metabolism occurred at the early stages of culturing and correlated to the displacement of fast (τ1) and intermediate (τ2) Maxwell elements. Fibroblasts seeded in low PA concentrations spread faster during 14 d than cells cultured in higher agarose concentrations. Collectively, these results confirm that PA viscoelasticity and hydrogel architecture strongly influenced cell behavior. Therefore, viscoelasticity is a key parameter in the design of PA-based implants.

1. Introduction

Hydrogel-based skin equivalents have emerged as the most promising approaches for skin tissue engineering (TE) applications due to their characteristics to mimic the native skin microenvironment by acquiring different shapes and incorporating cell populations [1,2].

One challenge faced by the use of hydrogels for skin TE applications is the ability to replicate the mechanical properties of the skin and its active (mechanical) stresses [1,3]. As most tissues within the body, the extracellular matrix (ECM) of the skin exhibits a combination of elasticity and viscosity, called viscoelasticity [4,5]. Elasticity is the physical property of a substance that allows changing its volume, length, or shape in response to a force, followed by recovery to its initial configuration once the force is removed. Viscoelasticity relates to the adaptability of the ECM network and the water content of the skin which adds flow or viscosity. In response to a constant deformation, viscoelastic materials exhibit stress relaxation in response to a constant strain [6]. The viscoelastic behavior of the skin protects against injury by allowing additional movement (as compared to pure elastic properties) of skin structures away from stress and returning toward their baseline without breaking [7].

Plasma-derived hydrogels (also referred to as fibrin hydrogels) are considered promising for skin TE applications because they are easily obtained from the patient's blood, providing a suitable alternative in clinical protocols of autologous use [8,9]. Furthermore, plasma-derived hydrogels offer additional advantages such as low cost and biocompatibility. Plasma-derived/fibrin hydrogels can be remodeled by cells and retain growth factors [10,11]. However, plasma-derived hydrogels are

* Corresponding author at: Antonius Deusinglaan 1, 9713AV Groningen, the Netherlands.
E-mail address: p.k.sharma@umcg.nl (P.K. Sharma).
[1] These authors contributed equally

https://doi.org/10.1016/j.bioadv.2022.212967
Received 10 February 2022; Received in revised form 26 May 2022; Accepted 31 May 2022
Available online 7 June 2022

not mechanically resilient, complicating their manipulation. Thus, several studies have already focused on improving their mechanical strength. For example, combining human plasma with other natural polymers such as agarose forms an interpenetrating network where both polymers are crosslinked simultaneously [12,13]. Agarose has a poroelastic structure, self-gelling properties, and high water content. These properties combined provide a suitable microenvironment for cellular activity [14,15]. Moreover, agarose hydrogels mechanics can be adjusted by changing the concentration, resulting in characteristics similar to the desired tissue. The potential of plasma-agarose (PA) interpenetrating polymer networks to produce biocompatible materials was demonstrated with multiple tissue models such as the cornea [16], oral mucosa [17], and neuronal tissue [18]. Nevertheless, there is limited knowledge about the effect of different concentrations of agarose on the viscoelastic behavior of PA hydrogels and the resulting cellular responses.

Agarose concentration can also modify the structural properties of hydrogels. Changes in hydrogel viscoelasticity and structure may impact cell spreading, growth, and proliferation in three-dimensional (3D) culture conditions [6,19].

In this study, we investigated the viscoelastic properties of PA hydrogels with different concentrations of agarose and determined the cellular responses of human dermal fibroblasts, and evaluated the potential use of these hydrogels for skin TE applications.

2. Methods

2.1. Cell culture

Human adult dermal fibroblasts (NHDF-Ad; Lonza, The Netherlands) passage 1, tested and certified as mycoplasma-free and virus-free (HIV-1, hepatitis B, and hepatitis C) were cultured in 75 cm^2 culture flasks with Dulbecco's modified Eagle's medium (DMEM; Thermo Fisher Scientific, USA) 25 mM glucose, supplemented with 10 % (*v*/v) fetal bovine serum (FBS; Gibco, USA) and 1 % (v/v) penicillin-streptomycin (Gibco). Cells were incubated at 37 °C, and 5 % CO_2 until these reached 80 % confluence. Passages between 2 and 6 were used for all experiments.

2.2. Hydrogel preparation

For the preparation of the PA hydrogels, a solution (1 mL) of platelet-poor human plasma (with a fibrinogen concentration of 2.5 mg/mL assessed by the Clauss fibrinogen assay This assay shows and SD of 0.7 mg/mL as reported in the literature [20,21]), 140 μL 150 mM NaCl, 14 μL of tranexamic acid (5 mg/mL) (CAS Number 1197-18-8, Sigma), and 40 μL of a fibroblast suspension (2.5 × 10 [5] cells/mL) was mixed with 0 %, 0.5 %, 1 %, 1.5 % or 2 % (*w*/*v*) of agarose type VII (CAS 9012366, Sigma, USA). The final concentrations of agarose in the PA hydrogels were adjusted by conveniently varying the plasma volumes (67 %–27 %). Before fibroblasts were added, 5 % (*w*/*v*) agarose was prepared, melted at 60 °C in 50 mL 150 mM NaCl and left overnight. Subsequently, the agarose stock solution was cooled to 37 °C and kept until used. To promote fibrin polymerization, 140 μL CaCl2 (1 %) (Sigma) were added to the PA hydrogel solution and gently homogenized. Then, 0.5 mL was poured into a 24-well plate (Corning, USA) and incubated in a humidified atmosphere with 5 % CO2, at 37 °C for 30 min. PA hydrogels with fibroblasts were cultured for 1 d, 7 d, and 14 d for the next experiments, and the culture medium was refreshed every other day. Cell-free hydrogels were also prepared.

2.3. Swelling ratio

Cell-free 0 %, 0.5 %, 1 %, 1.5 % or 2 % PA hydrogels were weighed 1 h after polymerization to determine their dry mass (*Md*). All hydrogels were swollen in 400 μL of phosphate-buffered saline (PBS; pH 7.4) for 24 h at 37 °C. The excess PBS from PA-hydrogels was removed with blotting paper before being weighed again to determine the wet mass (*Mw*). The mass swelling ratio was quantified according to Eq. (1): [22]

$$\text{Mass swelling ratio} = \frac{Mw}{Md} \tag{1}$$

2.4. Viscoelastic properties

The viscoelastic properties of cell-loaded and cell-free PA hydrogels were determined using uniaxial compression on a low-load compression tester (LLCT) [23,24]. PA hydrogels of 2.0 ± 0.4 mm thick were placed on a glass coverslip with double-sided tape to prevent sample displacement. Each PA hydrogel was compressed at a constant strain rate of 0.2 s^{-1} to 80 % of its original thickness (strain, $\varepsilon = 0.2$) with a 2.5 mm diameter steel plunger and kept compressed for 100 s. Strain (ε) was calculated as the change in thickness during compression normalized with the starting gel thickness. Force output from the LLCT was normalized by the area of the cross-section of the plunger to get stress (σ). All data were analyzed with a data fitting routine written in MatLab 2018 (MathWorks® Inc., Natick, USA). The elastic modulus was calculated as the slope of the stress-strain curve (Fig. 1a) while the stress relaxation was calculated by comparing initial stress ($t = 0$ s) versus final stress ($t = 100$ s) (Fig. 1d).

During the stress relaxation, $E(t)$ was defined as a time-dependent elastic modulus, where σ(t) is the measure of time-dependent stress (Fig. 1d) and ε_o the constant strain value of 0.2 (Fig. 1c), decreasing with time t during 100 s according to Eq. (2):

$$E(t) = \frac{\sigma(t)}{\varepsilon_o} \tag{2}$$

The measured stress relaxation curves were modeled using a generalized Maxwell model (Fig. 1e, f) by fitting Eq. (3):

$$E(t) = E_1 e^{-\frac{t}{\tau_1}} + E_2 e^{-\frac{t}{\tau_2}} + E_3 e^{-\frac{t}{\tau_3}} + \ldots E_i e^{-\frac{t}{\tau_i}} \tag{3}$$

where $\tau_i = \eta_i / E_i$ is the relaxation time constant, η_i the viscosity, and E_i the spring constant for each Maxwell element i. Using this formula, the number of Maxwell elements for each hydrogel could be calculated.

The optimal number of Maxwell elements required was determined using the Chi-square function (Fig. 1g) following Eq. (4):

$$x^2 = \sum_{j=0}^{100} \left[\frac{E_j - E(t_j)}{\sigma_j} \right] \tag{4}$$

where j varies from 0 to 100 s, E_j is the measured value at time j, $E(t_j)$ is calculated from Eq. (3) and σ_j is the standard error of the device equal to 1.41 Pa.

2.5. Cell number and cell morphology

Cell number and morphology of fibroblasts loaded cultured in PA hydrogels were analyzed by fluorescence microscopy at 1 d, 7 d, and 14 d. To visualize the expression of filamentous actin (F-actin) and nuclei, FITC-labeled phalloidin (Sigma) and 4′, 6-diamidino-2-phenylindole (DAPI; D9564, Sigma,) were used, respectively. PA hydrogels were washed with PBS, fixed with 3.7 % paraformaldehyde (PFA; Sigma) diluted PBS for 1 h, and subsequently washed again three times. Afterward, fixed hydrogels were permeabilized using 0.5 % (*v*/v) Triton X-100 - PBS solution for 3 min and blocked with 5 % bovine serum albumin in PBS for 30 min. FITC-labeled phalloidin (2 μg/mL) was applied and incubated for 30 min at room temperature, light protected. DAPI (4 μg/mL) was then added to stain the cell nuclei and incubated for an additional 1 h. After staining, PA hydrogels were visualized with a Leica DMR fluorescence microscope (Leica, Wetzlar, Germany), and ≥ 10 areas per hydrogel were imaged for cell counting. Three independent samples were analyzed per PA concentration.

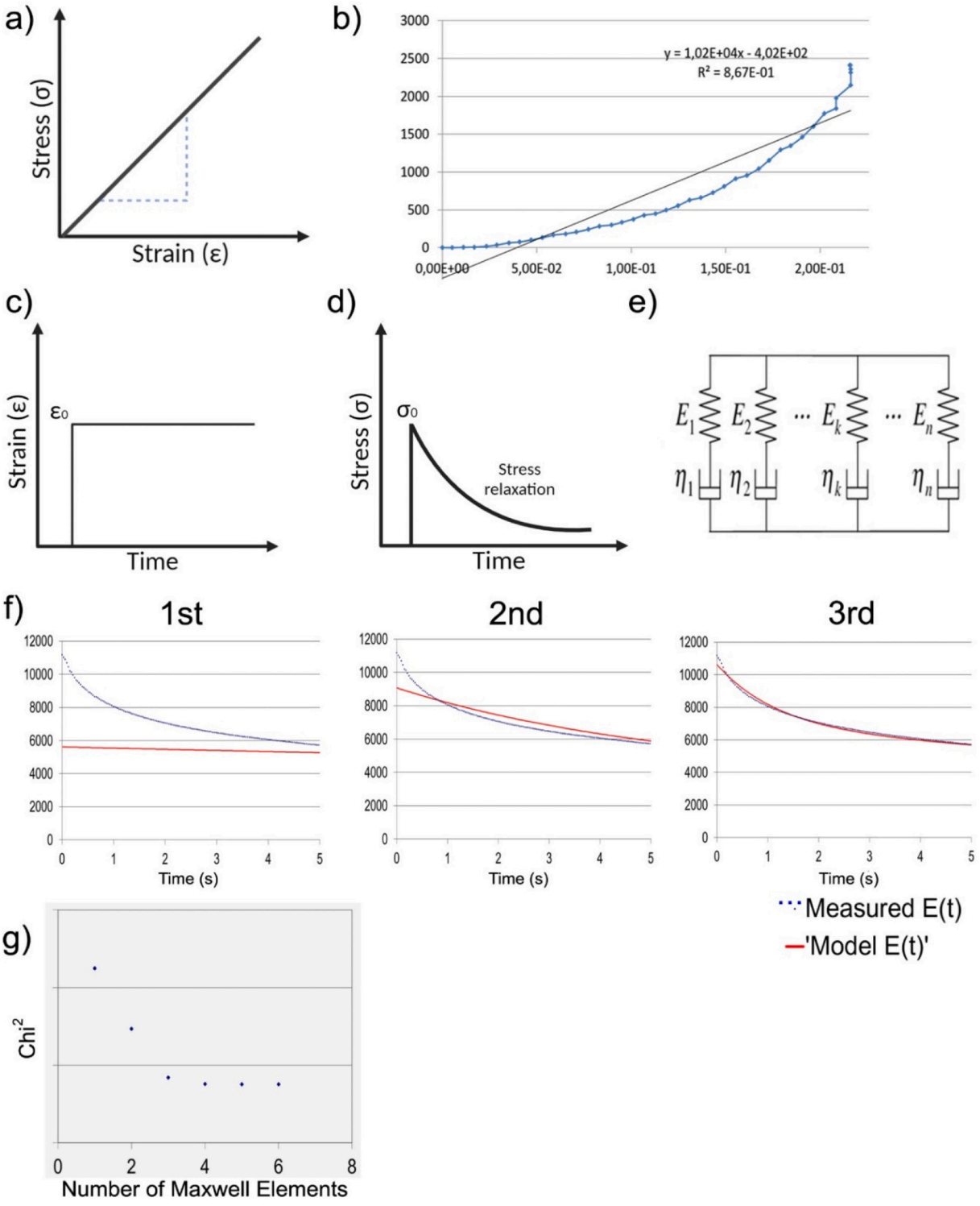

Fig. 1. Elastic modulus and stress relaxation. a) The elastic modulus is the slope of the stress-strain curve. b) Elastic modulus for the real data was taken as the slope of the least squared fit line, shown here for PA 2 % hydrogel is shown c) For a stress relaxation test, a constant strain is applied, and d) the decrease (relaxation) in stress over time detected by the low-load compression tester. e) The stress relaxation data were analyzed by fitting a generalized Maxwell model. f) Example of Maxwell analysis derived from a PA 2 % hydrogel, shows the curve fitting based on the measured modulus *E(t)* and the model *E(t)*. g) The number of necessary Maxwell elements was decided based on the Chi [2] minimization.

2.6. Cell metabolic assay

Cell metabolic activity of cell-loaded PA hydrogels was based on a mitochondrial activity assay as previously described [25]. Briefly, 500 μL of XTT ((2,3-bis (2-methoxy-4-nitro-5-sulfophenyl)-2H-tetrazo-lium-5-carboxanilide salt; A8088 AppliChem, The Netherlands) was mixed with the culture medium present on top of each hydrogel and incubated at 37 °C, 5 % CO_2 for 6 h. The absorbance was measured at 460 nm and 690 nm using a microplate reader (Shimadzu, Japan). The resulting metabolic activity (%) of all PA hydrogels was compared to the values of

0 % PA hydrogels based on Eq. (5).

$$\text{Metabolic activity } (\%) = \frac{A_{PA\ hydrogel}460\ \text{nm} - A_{PA\ hydrogel}690\ \text{nm}}{A_{0\%PA\ hydrogel}460\ \text{nm} - A_{0\%PA\ hydrogel}690\ \text{nm}} \times 100 \quad (5)$$

The absorbance of all PA hydrogels was corrected by subtracting the background absorbance from cell-free hydrogels of their respective concentrations at 1 d, 7 d, and 14 d.

2.7. Ultrastructure

The ultrastructure of cell-loaded and cell-free PA hydrogels, defined as the architectural properties at the micrometer scale, were characterized with scanning electron microscopy (SEM; Jeol JSM 6490 LV, USA) at 1 d. All hydrogels were sectioned in half to visualize the internal ultrastructure, then fixed in 3 % glutaraldehyde diluted in PBS (pH 7.4) for 24 h followed by 1 % electron microscopy grade osmium tetroxide for 1.5 h. Afterward, the hydrogels were dehydrated in a series of ethanol concentrations (30 %, 50 %, 70 %, 90 %, 95 %, and 99 %), critical point dried at 31 °C, 1072 PSI, and Au sputter coated (Denton Vacuum Desk IV). The SEM imaging occurred under a high vacuum at 15 kV and 5000× magnification. SEM images were employed to calculate the porosity percentage and fiber thickness with ImageJ Ver 1.52p (https://imagej.nih.gov/ij/; Accessed: 12 October 2021).

2.8. Histological analysis of collagen

Cell-loaded PA hydrogels at 7 d were fixed with 3.7 % PFA (Sigma). Fixation occurred for 24 h at 4 °C, then dehydrated in a series of ethanol concentrations and paraffin-embedded. Sections (5 μm) were made with a microtome (Leica RM2265, Germany), stained with Masson's trichrome (ab150686, Abcam) according to the manufacturer's instructions, and imaged with Leica DMR. Cell-free hydrogels and human skin sections (5 μm) kindly donated by the Tissue Engineering and cell therapy research Group of the University of Antioquia were also stained. Only the dermal layer of the skin was considered for comparison with PA hydrogels. The collagen positive area was quantified using the ImageJ software in three fields of view captured from each PA hydrogel. The blue positive area was divided by the total area for each field, and the result was expressed as the percentage of collagen deposition relative to native skin.

2.9. Statistical analysis

All data are expressed as mean values ± standard deviation. Statistical analysis was performed with OriginPro 2018 (v9.5.1). Data were checked for normality according to Kolmogorov-Smirnoff and for outliers using the robust regression and outlier removal test (ROUT). Data were analyzed using one-way or two-way ANOVA followed by Tukey's test to determine differences between groups $^{*}p < 0.05$, $^{**}p < 0.01$, $^{***}p < 0.001$, and $^{****}p < 0.0001$, respectively. Correlations between the increase in agarose concentrations and the variables of viscoelasticity and cellular response were determined by Pearson's (r) coefficient. Values between 0.70 and 1 (−0.70 to −1) were considered high, and between 0.50 and 0.70 (−0.50 to −0.70) were considered moderate, positive (negative) correlations.

3. Results

3.1. Swelling

The swelling ratio of cell-free 0 %, 0.5 %, 1 %, 1.5 %, and 2 % PA hydrogels is shown and compared in Fig. 2. The 0 % PA hydrogels had a lower swelling ratio than 1 %, 1.5 %, and 2 %. Hydrogels of 0.5 % PA also had a lower swelling ratio than 2 %. Comparison between 1 %, 1.5 %, and 2 % PA hydrogels showed no differences. The addition of agarose led to an increase in swelling ratio, albeit, this increase became non-linear at higher agarose concentrations (<1.5 %).

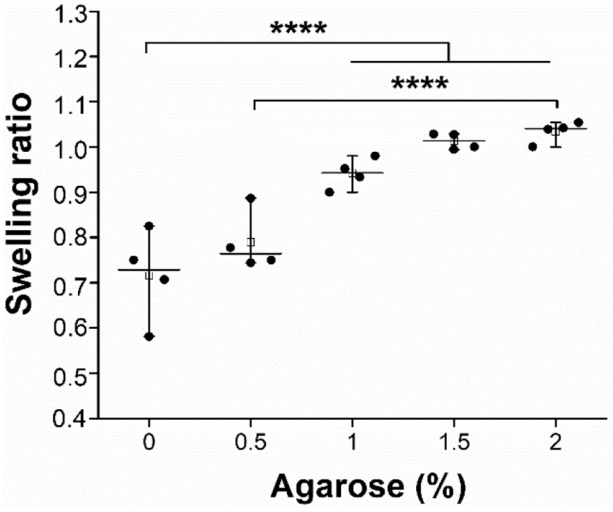

Fig. 2. Swelling behavior of 0 %, 0.5 %, 1 %, 1.5 % and 2 % PA (*w/v*). The swelling ratio was assessed after swelling all hydrogels in PBS for 1 d at 37 °C and then dried for 1 h at 37 °C. Data show the mean values and the standard deviation ($n = 4$). One-way ANOVA followed by Tukey's honestly significant difference (HSD) test: **** $p < 0.0001$.

3.2. Viscoelastic properties

Cell-loaded and cell-free PA hydrogels had an agarose concentration-dependent increase in elastic modulus (stiffness) (Table 1). Overall, fibroblasts did not alter the elastic modulus of the PA hydrogels at any time point. All PA concentrations decreased in stiffness regardless of cells' presence over time. These results demonstrate that the stiffness of plasma-derived hydrogels is tunable by increasing the agarose concentration.

Irrespective of the PA ratio or the presence of cells, all hydrogels had a similar stress relaxation (Table S1).

3.3. Maxwell analysis

PA hydrogels required three Maxwell elements to describe their stress relaxation (Fig. 3), defined as fast (τ1), intermediate (τ2), and slow elements (τ3). The number of Maxwell elements remained the same during the 14 d of experimental conditions, regardless of cell presence.

To further evaluate the viscoelastic behavior of PA hydrogels in response to increased agarose concentrations, Pearson's correlation coefficients (r) of hydrogels after 1 d, 7 d, and 14 d in culture were analyzed. Fig. 4 shows a high positive correlation between the relaxation τ1) and τ2, and the increase in agarose concentrations at all evaluated time points, while τ3 did not correlate with the agarose content.

3.4. Cell behavior

Cellular (fibroblast) morphology was assessed in PA hydrogels via Phalloidin and DAPI fluorescent stains at 1 d, 7 d, and 14 d of 3D cell culture. Representative images are shown in Fig. 5a. The expression of F-actin (green) filamentous extensions was the highest at the lower PA hydrogel concentrations. The typical spindle-shaped morphology of fibroblasts was predominant in 0 % and 0.5 % hydrogels at all time points. In 1 % PA hydrogels, cells expressed F-actin but were only visible after 14 d. F-actin was not detected in 1.5 % and 2 % PA hydrogels.

The number of cells was calculated based on the number of DAPI positive particles (i.e. nuclei) and compared to 0 % PA hydrogels.

Table 1
Elastic modulus (kPa) of cell-loaded and cell-free PA hydrogels at 1 d, 7 d, and 14 d.

Timepoint	Agarose (%) in the PA hydrogel									
	0 %[(a)]		0.5 % [(b)]		1 %		1.5 %		2 %	
	Cell-free	Cell-loaded	Cell-free	Cell-loaded	Cell-free	Cell-loaded	Cell-free	Cell-loaded	Cell-free	Cell-loaded
1 d	0.64 ± 0.06	0.51 ± 0.03	1.51 ± 0.52	1.46 ± 0.23	5.24 ± 0.80[a]	2.84 ± 1.02[b]	14.40 ± 2.66[a]	15.09 ± 10.24[b]	15.57 ± 7.06[a]	13.78 ± 7.26[b]
7 d	0.99 ± 0.05[a]	0.49 ± 0.19[a]	0.96 ± 0.32[a]	0.42 ± 0.19[a]	1.65 ± 0.21[a]	1.15 ± 0.30[b]	6.94 ± 2.05[a]	7.51 ± 1.51[b]	11.10 ± 0.82[a]	1.27 ± 0.24[b]
14 d	0.76 ± 0.12[a]	0.27 ± 0.04[a]	0.62 ± 0.33[a]	0.89 ± 0.24[a]	0.92 ± 0.02[a]	3.16 ± 0.73[b]	5.58 ± 2.85[a]	3.74 ± 0.86[b]	4.93 ± 3.32[a]	2.07 ± 0.55[b]

[a] Indicates significance compared to 0 % PA cell-free hydrogels.
[b] Indicates significance compared to 0 % PA cell-loaded hydrogels. Data derive from three independent non-paired samples per time point. Data are shown as mean values and standard deviation and analyzed with Two-way ANOVA followed by Tukey's HSD test of values $p < 0.001$.

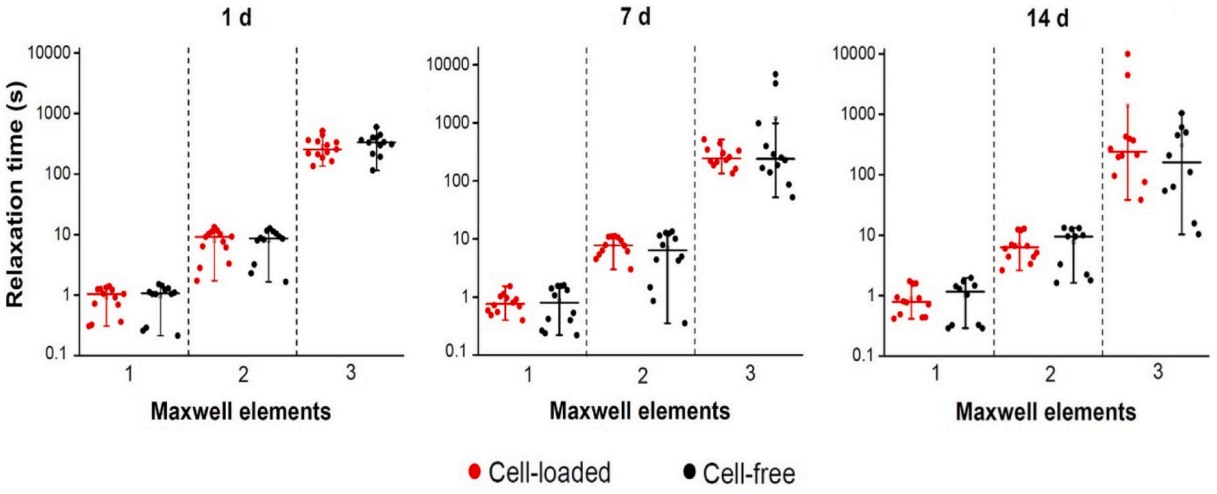

Fig. 3. Relaxation time constants of Maxwell elements for cell-loaded (Red) and cell-free (Black) PA hydrogels (all agarose concentrations). No differences were observed between cell-loaded and cell-free hydrogels at the same timepoint. Data derive from three independent non-paired samples per time point. Data are shown as mean values and standard deviation. (For interpretation of the references to color in this figure legend, the reader is referred to the web version of this article.)

Quantification indicates that the number of cells decreased as agarose concentration increased. The 0 % PA hydrogels had a greater number of cells than all the other concentrations at any given time point (Fig. 5b).

The metabolic activity per cell was calculated with Eq. (5) and indicated that cells in 1.5 % and 2 % PA hydrogels had higher metabolic activity than 0 % PA at 7 d and 14 d (Fig. 5c).

3.5. Ultrastructure

The ultrastructure of cell-free PA hydrogels was determined with SEM by analyzing the porosity (%) and fiber diameter at 1 d. Representative images are shown in Fig. 6. SEM evaluation of the 2 % PA hydrogels was unfeasible due to brittleness and fracture during processing. The porosity of all hydrogels decreased with increasing agarose concentrations (Fig. 6c), while the fiber thickness was greater in 0.5 % PA hydrogels than in 0 % and 1 % hydrogels. Analysis of 1.5 % PA hydrogels derived no fiber diameter data, due to the high polymer density.

3.6. Histological analysis of collagen deposition

The presence of cell-derived collagen was evaluated by Masson's Trichrome stain in cell-loaded and cell-free PA hydrogels. Native human skin was used for comparison and as a staining control. Representative images are shown in Fig. 7. All PA hydrogels had areas positively (blue) stained for collagen. The 0 % and 0.5 % PA hydrogels had areas of clustered cells and similar stain (color) intensity to the dermal layer of native skin. In the 1 % PA hydrogels, positively-stained collagen (blue) regions were less dense than in 0 % and 0.5 % PA. In 1.5 % and 2 % PA fewer cells were visible, and the collagen deposition was minimal, compared to the before-mentioned hydrogel concentrations. All cell-free hydrogels showed a similar staining and color intensity pattern. Quantification of the color intensity of positively-stained collagen (blue) showed that of 0 %, 0.5 % and 1 % PA hydrogels did not differ from native skin (dermis layer). In contrast, 2 % PA and cell-free hydrogels had a lower intensity compared to the dermis layer of native skin.

3.7. Correlations between the viscoelastic properties and cell behavior

The addition of agarose to plasma-derived hydrogels correlated with mechanical and structural changes. The exact values are shown in Table 2. The stiffness, $\tau 1$, $\tau 2$, and fiber diameter positively correlated with the increase in agarose concentration. Meanwhile, cell number, metabolic activity, and porosity negatively correlated to the increase in agarose. The metabolic activity positively correlated with the number of cells, while fiber diameter, $\tau 1$, and $\tau 2$ negatively correlated with such. Porosity negatively correlated with the number of cells and the $\tau 1$ and $\tau 2$ values. The analysis of the influence of $\tau 1$ and $\tau 2$ on the cellular parameters can be found in Fig. S1.

4. Discussion

In this study, we characterized the viscoelastic properties of plasma-agarose (PA) hydrogels produced with varying concentrations of

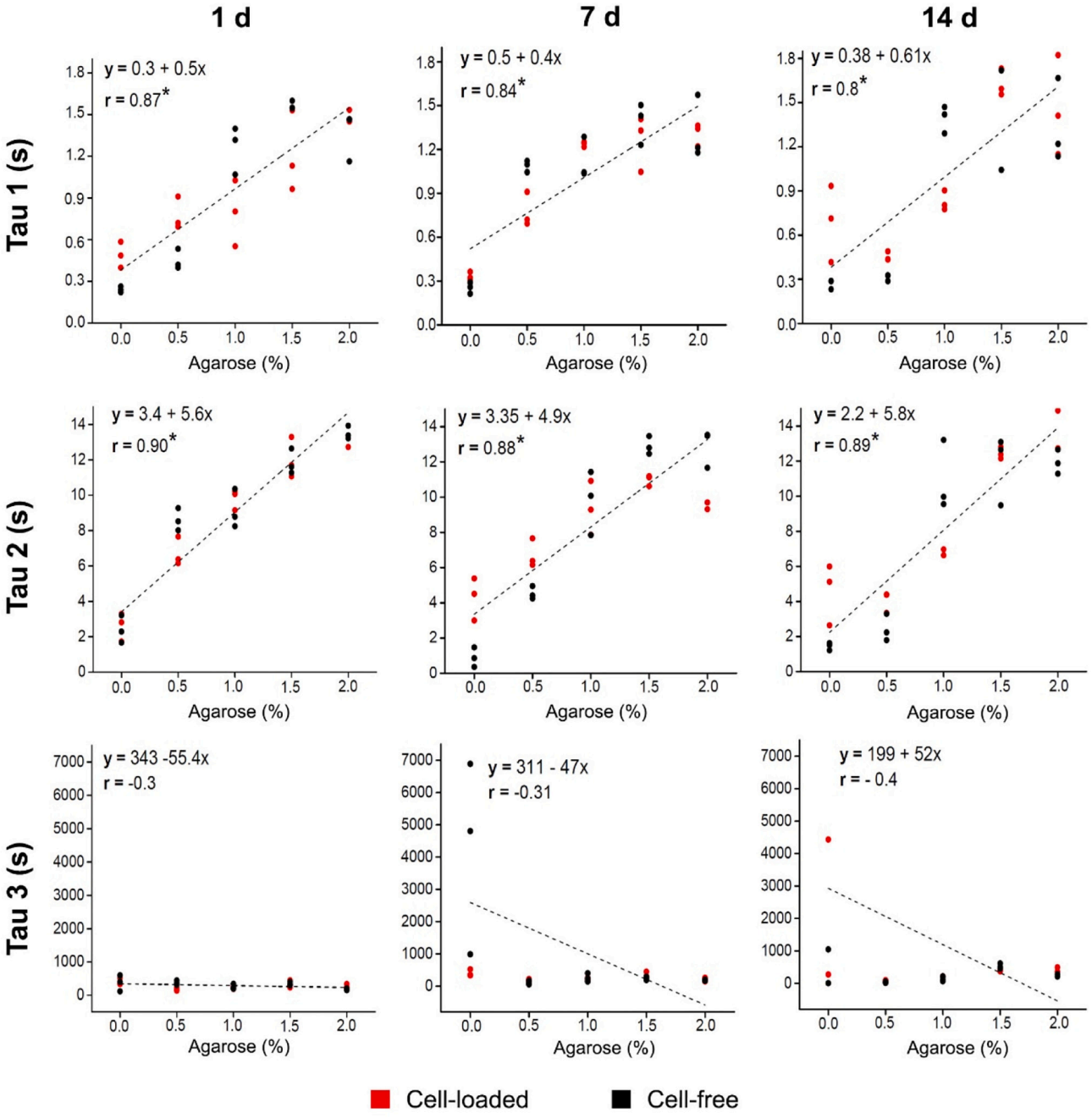

Fig. 4. Correlations between the relaxation time constants tau 1 (τ1), tau 2 (τ2), and tau 3 (τ3) as a function of agarose concentrations at 1 d, 7 d, and 14 d. Cell-loaded (red) and cell-free (black) were analyzed together as no differences were found among the two conditions as shown in Fig. 3. (For interpretation of the references to color in this figure legend, the reader is referred to the web version of this article.)

agarose and the response of loaded human dermal fibroblasts. The elastic modulus and stress relaxation properties, together with the ultrastructural parameters and cell responses were investigated to determine the potential use of these hydrogels for skin TE applications.

Viscoelasticity is a near-universal property of living tissues and their extracellular matrix (ECM) [8] manifested as stress relaxation or creep under compression or tension. A thorough understanding of this mechanical behavior is relevant for an adequate design of human skin equivalents. In the context of skin TE, fibrin hydrogels are widely employed due to their biological properties [26]. However, the native mechanics of plasma, and its main constituent fibrin makes them unsuitable to withstand the mechanical stresses to which skin is constantly exposed. Here, we produced human plasma-derived hydrogels from pooled plasma containing a fibrinogen concentration of 2.5 mg/mL, which has been associated with low rates of cell-mediated contraction and a shelf life >18 days [28].

Under uniaxial compression, the 0 % PA-hydrogels showed an instantaneous elastic response followed by stress relaxation. The 0 % PA hydrogels reached 50 % stress relaxation in 55.1 ± 2.8 s, while agarose addition did not affect the overall relaxation process. The irreversible rearrangement of fibrin to relieve stress is related to the knob:hole non-covalent interactions that hold the fibrin network together. Such knob: hole bonds can break and re-form within the PA network after stress is released [27,29,30]. Other hydrogel systems, such as type-1 collagen and basement membrane also exhibit viscoelastic behavior, unless they are sufficiently covalently crosslinked. Such stability can be achieved by

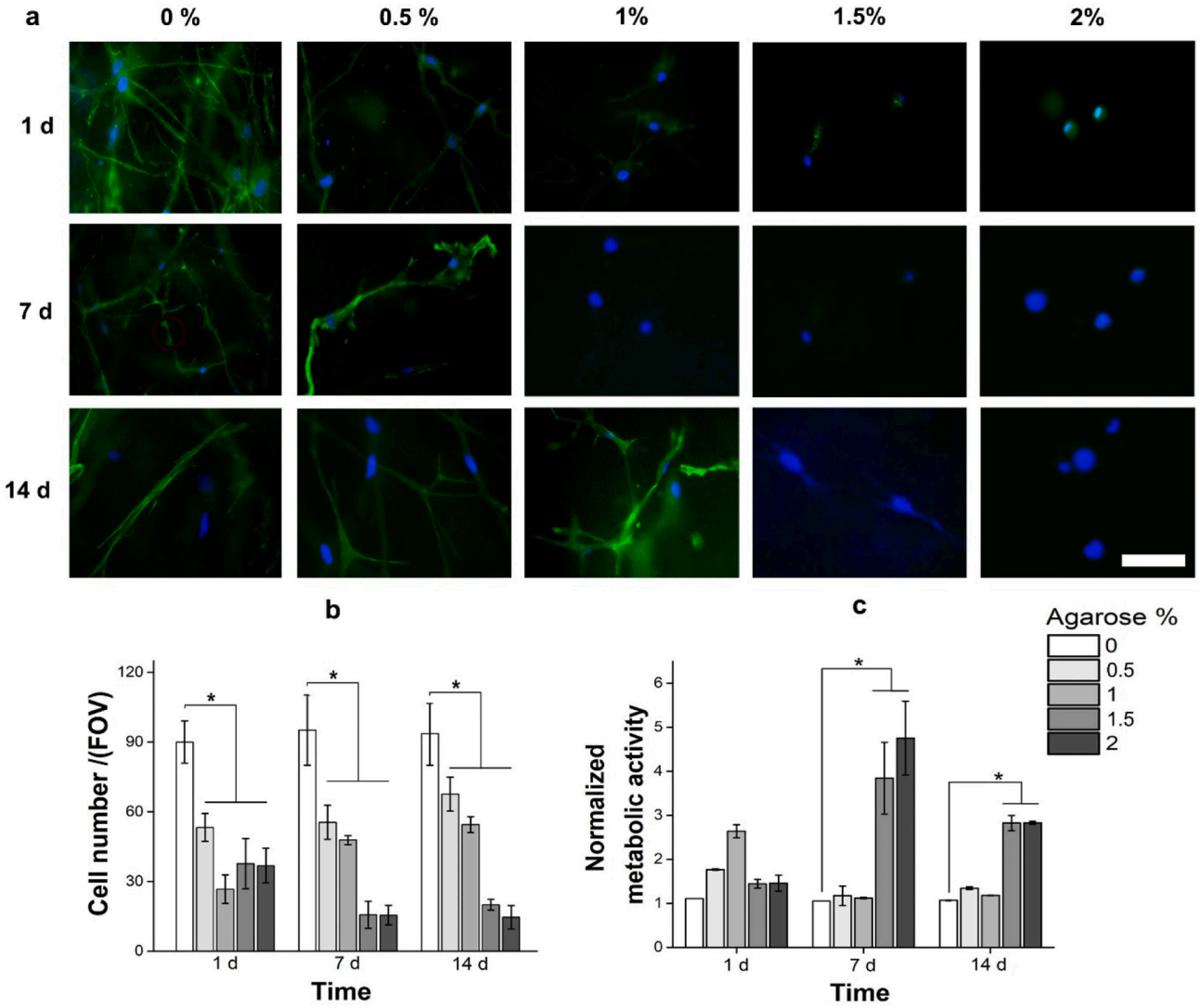

Fig. 5. Cell morphology, number of cells, and metabolic activity (normalized) at 1 d, 7 d, and 14 d. (a) The morphology of cells (fibroblast) according to DAPI (blue) and F-actin (green) fluorescent stains within 0 %, 0.5 %, 1 %, 1.5 % and 2 % PA hydrogels. The scale bar represents 20 μm. (b) The number of cells according to the number of DAPI positive particles (i.e. nuclei). A total of 10 fields of view (FOV) were analyzed per condition. (c) Metabolic activity per cell according to XTT assay. Absorbance was normalized with cell-free PA hydrogels and compared to 0 % PA hydrogels. Data derive from three independent non-paired samples per time point. Data are shown as mean values and standard deviation and analyzed with Two-way ANOVA followed by Tukey's HSD test of values * $p < 0.05$. (For interpretation of the references to color in this figure legend, the reader is referred to the web version of this article.)

combining these natural polymers with others regarded as more mechanically stable and modifying their crosslinking [31–33].

Based solely on the time to reach 50 % stress relaxation, the addition of agarose to fibrin hydrogels seemingly had no impact on hydrogel viscoelasticity. Nonetheless, Maxwell's modeling of the stress relaxation data showed a strong positive correlation between the agarose concentration and the τ_1 and τ_2. Viscoelastic stress relaxation is caused by various molecular events taking place inside the hydrogel, that include the dissociation of the network bonds within the matrix and fluid movement through its pores. Changes in hydrogel composition could change the relaxation time constants and the relative importance of particular Maxwell elements. In the absence of a systematic study linking particular Maxwell elements to the hydrogel biochemical composition, the exact allocation of components to particular Maxwell elements remains a hypothetical exercise. A systematic study performed on bacterial biofilms [34] demonstrated that smaller molecules (e.g. unbound water, bound water, growth factors) responded to the applied strain faster and to Maxwell elements with smaller relaxation time constants. The increase in agarose concentration was followed by an increase in τ1 and τ2 and may relate to agarose hygroscopic properties. Increasing agarose concentration increased the PA hydrogel swelling ratio increasing the relative amount of bound water and decreasing its mobility under stress. The resistance to the movement of bound and unbound water could cause an increase in τ1 and τ2. However, τ3 might correspond to the structural components such as the primary fibrin network present in all PA hydrogels, but further research is needed to properly identify the components active in this Maxwell element.

Since the mass of hydrogels consists mostly of water, the swelling capacity of PA hydrogels and their relationship with the network porosity was evaluated. The 0 % PA hydrogels showed a de-swelling behavior that has been previously reported [28], likely due to the typical contraction of these hydrogels leading to protein release. Compared to 0 %, the 1 % PA hydrogels had increased their mass after swelling in PBS. Agarose is hygroscopic, making this result expected and preventing volume loss. Other authors reported that 0.1 % and 0.5 % PA hydrogels were 1.5 and 2.0 times thicker than hydrogels made from only plasma (0 % PA) [35].

Agarose concentration influenced the viscoelastic properties of PA

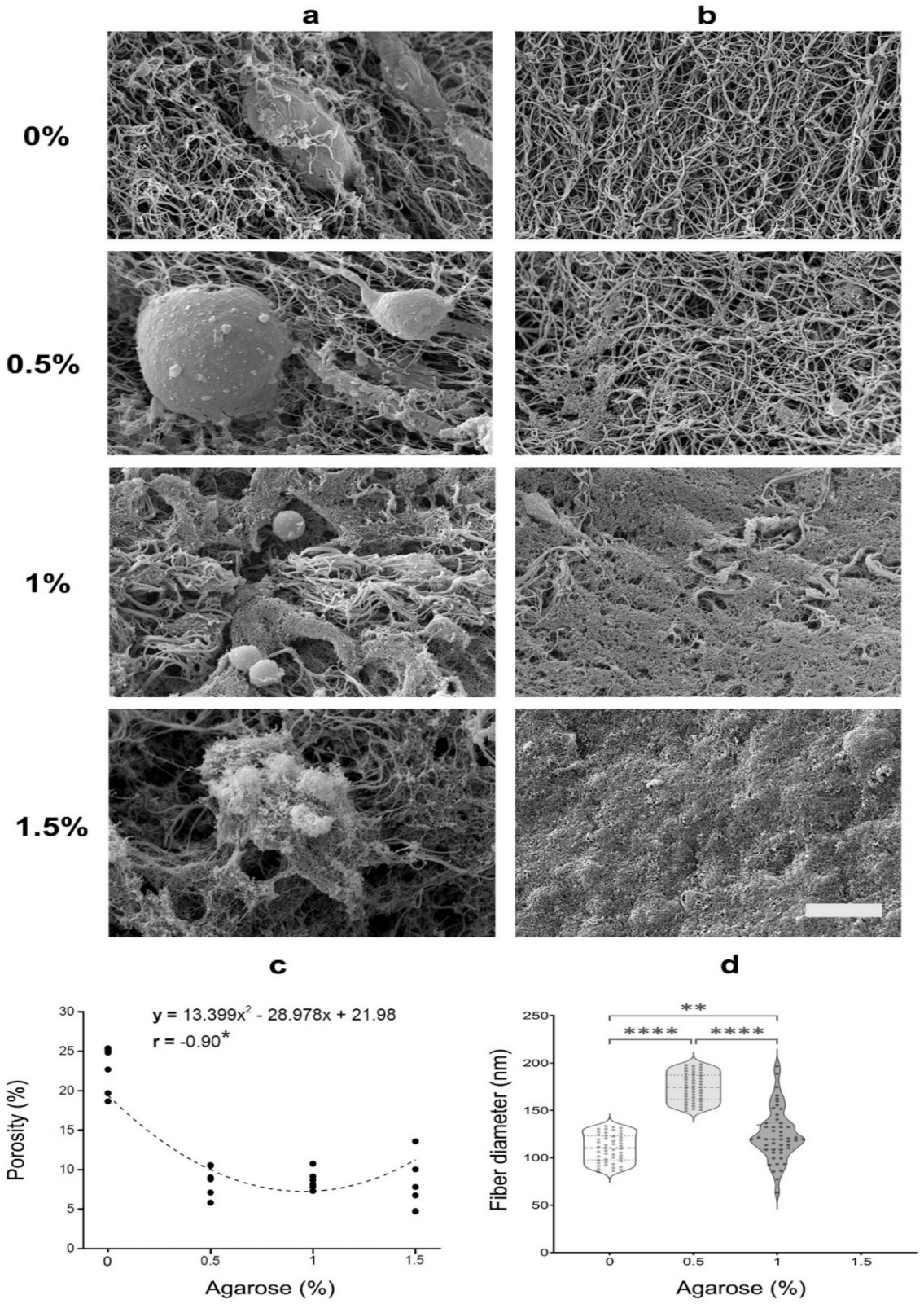

Fig. 6. Representative SEM micrographs showing the ultrastructure of (a) cell-loaded and (b) cell-free 0 %, 0.5 %, 1 %, and 1.5 % PA hydrogels at 1 d. Scale bars represent 5 μm. (c) Correlation between porosity (%) of PA hydrogels as a function of increasing concentrations of agarose after 1 day. Data derived from a minimum of three independent experiments.

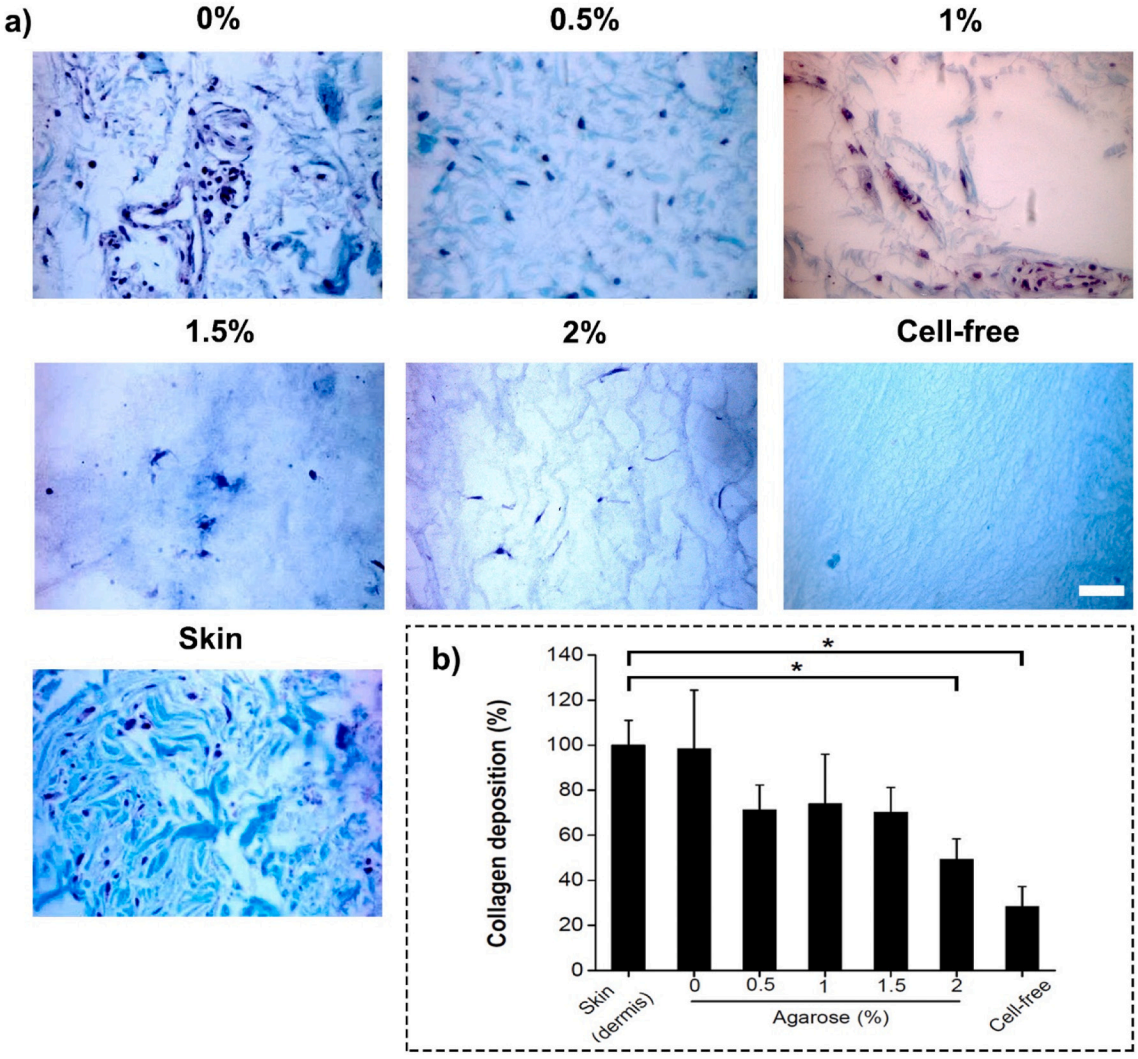

Fig. 7. Collagen deposition. (a) Histology of cell-loaded PA hydrogels. Cell-free and native skin are shown as controls of the Masson's trichrome stain. Scale bars represent 50 μm. (b) Collagen deposition in PA hydrogels relative to the skin (dermis). Data represent mean values and standard deviation and were analyzed with Two-way ANOVA followed by Tukey's HSD test of values * $p < 0.05$.

Table 2
Pearson's correlation coefficients analysis.

Variables	Agarose (%)	Metabolic activity (%)	Cell number/ (FOV)	Porosity (%) (SEM)
Metabolic activity (%)	−0.87[a]			
Cell number/ (FOV)	−0.90[a]	0.80[a]		
Porosity % (SEM)	−0.91[a]	0.46	0.76[a]	
Stiffness (KPa, 0.2 s^{-1})	0.65[a]	−0.44	−0.44	−0.43
Fiber diameter (nm) (SEM)	0.67[a]	−0.64[a]	−0.68[a]	−0.28
τ1	0.84[a]	−0.69[a]	−0.73[a]	−0.86[a]
τ2	0.90[a]	−0.68[a]	−0.65[a]	−0.83[a]
τ3	−0.36	0.31	0.36	0.42

[a] Correlation positive/negative.

hydrogels and strongly correlated with a lower number of cells and negatively correlated with the cell metabolic activity. In other hydrogel systems, increasing polymer concentration seems to be detrimental for cells in long-term 3D culture [36,37]. However, the metabolic activity normalized by cell number showed increased mitochondrial activity in 1.5 % and 2 % PA hydrogels, perhaps due to the challenge the cells experience to survive under adverse conditions such as low availability of nutrients or hypoxia [38].

The highest negative correlations between τ1 and τ2 and the number of cells occurred after 1 d, indicating that the main changes in cell responses happened in the early stages of culturing and were related to the displacement of fast (τ1) and intermediate (τ2) Maxwell elements as shown in the Fig. S1.

One of the parameters affected by increasing agarose concentration was the hydrogel porosity. The porosity and pore sizes are key regulators for mechanical confinement in 3D cultures. Cell spreading and cell migration are hindered in materials with small and rigid pores, preventing the movement of the cell's nuclei [6,39]. The PA hydrogels with lower agarose concentrations had greater cell spreading since 1 d, compared to those with higher agarose concentrations. Cell viability and spreading are positively correlated with high porosity (%) as it facilitates both processes while lower porosity (%) hinders them. These findings go per the existing literature in hydrogel culture systems [40,41]. and in our observations where fibroblast in 1 % PA took 14 d to show any signs of cell spreading. Hydrogel degradation matrix could allow the cells to overcome confinement, spread, and migrate [42]. Hence, the cell-induced degradation in vitro of PA hydrogels should be explored in

the near future [43].

The ECM is constantly remodeled by the cells within, causing a restructuring of tissue architecture. In our model, fibroblast-derived collagen deposition was observed in 0 %, 0.5 %, and 1 % PA-hydrogels, resembling that observed in native skin. This observation is promising for skin TE applications. Furthermore, the stiffness of 1 % PA hydrogels was similar to that reported in the skin (4.5–8 kPa) [28,44]. TE implants should pose similar mechanics to those found in the tissue aimed for repair [45]. Based on our data, the 1 % PA hydrogels are the most suitable candidates for skin TE applications, outperforming the other concentrations. The limitations of this study should be recognized. Dehydration of hydrogels for SEM analysis can lead to shrinkage and densification of the sample [46]. Hence, the visualized ultrastructure might not reflect the hydrogel in the swollen state. Therefore, the SEM-generated data is useful as a comparative measure as all hydrogels followed the same fixation and dehydration protocol. Cell viability was not assessed through conventional (fluorescent) methods previously reported in other hydrogels due to plasma autofluorescence [47]. Other biological events such as cell migration were not assessed since the 3D distribution of cells impedes tracking the same microscopy focal plane over time. PA hydrogels are viscoplastic that can undergo irreversible deformation on the microscale [48]. Such viscoplasticity is relevant to any biomaterial constantly exposed to mechanical stress and could be related to the decrease in PA hydrogel stiffness observed [48]. Hence, the determination of the viscoplasticity of hydrogels should be considered in future studies. A limitation of LLCT is that a constant strain rate allowed to determine the stress relaxation time, but does not serve to identify strain rate-dependent phenomena. Additional limitations of LLCT have been discussed in the past by our research group [36,49] Other mechanical tests, such as tensile tests would provide additional characterization of the robustness of the PA hydrogels for dermal applications. However, 20 % strain under tensile conditions would cause the failure of the hydrogel, and would not allow a proper assessment of cell-hydrogel viscoelasticity.

CRediT authorship contribution statement

M.I.P.V (Conceptualization, methodology, investigation, data curation, visualization, formal analysis, writing—original draft preparation). F.D.M.G (Investigation, visualization, data curation, formal analysis, writing—original draft preparation). F.O., and N.Y.B (Methodology, investigation). L.M.R., H.C.v.d.M., and M.C.H (Conceptualization, supervision, writing-review, and editing). T.G.v.K and P.K.S (Supervision, Resources, software and validation, formal analysis, writing,-review and editing). M.I.P.·V and F.D.M.-G. contributed equally to this work.

Funding

M.I.P.V. was supported by the Abel Tasman Talent Program (ATTP) of the University of Groningen, and the Colombian Administrative Department of Science, Technology and Innovation Doctoral program (COLCIENCIAS; code 727-2015). F.D.M.G and M.C.·H acknowledge the support of the Mexican National Council of Science and Technology (CONACyT; CVU-695528).

Declaration of competing interest

The author(s) declared no potential conflicts of interest concerning the research, authorship, and/or publication of this article. The funders had no role in the design of the study; in the collection, analyses, or interpretation of data; in the writing of the manuscript, or in the decision to publish the results.

Acknowledgments

The authors acknowledge the support of Gert ten Brink in the preliminary SEM imaging. We acknowledge the support of Janette K. Burgess for her helpful review of this manuscript.

Appendix A. Supplementary data

Supplementary data regarding the time to 50% stress relaxation and correlation between Maxwell Analysis with metabolic activity and cell number from this article can be found online at https://doi.org/10.1016/j.bioadv.2022.212967.

References

[1] S. Tavakoli, A.S. Klar, Advanced hydrogels as wound dressings, Biomolecules 10 (2020) 1169.
[2] K. Vig, et al., Advances in skin regeneration using tissue engineering, Int. J. Mol. Sci. 18 (2017) 789.
[3] I.M. El-Sherbiny, M.H. Yacoub, Hydrogel scaffolds for tissue engineering: progress and challenges, Glob. Cardiol. Sci. Pract. 2013 (2013) 38.
[4] J.S. Everett, M.S. Sommers, Skin viscoelasticity, Biol. Res. Nurs. 15 (2013) 338–346.
[5] M.-M. Constantin, et al., Measurement of skin viscoelasticity: a non-invasive approach in allergic contact dermatitis, Exp. Ther. Med. 20 (2020), 1-1.
[6] O. Chaudhuri, J. Cooper-White, P.A. Janmey, D.J. Mooney, V.B. Shenoy, Effects of extracellular matrix viscoelasticity on cellular behaviour, Nature 584 (2020) 535–546.
[7] N.T. Clancy, G.E. Nilsson, C.D. Anderson, M.J. Leahy, A new device for assessing changes in skin viscoelasticity using indentation and optical measurement, Skin Res. Technol. 16 (2010) 210–228.
[8] M.C. Catoira, L. Fusaro, D. Di Francesco, M. Ramella, F. Boccafoschi, Overview of natural hydrogels for regenerative medicine applications, J. Mater. Sci. Mater. Med. 30 (2019) 115.
[9] O. Moreno-Arotzena, J. Meier, C. del Amo, J. García-Aznar, Characterization of fibrin and collagen gels for engineering wound healing models, Materials (Basel) 8 (2015) 1636–1651.
[10] C. Wong, E. Inman, R. Spaethe, S. Helgerson, Fibrin-based biomaterials to deliver human growth factors, Thromb. Haemost. 89 (2003) 573–582.
[11] M. Dietrich, et al., Fibrin-based tissue engineering: comparison of different methods of autologous fibrinogen isolation, Tissue Eng.C Methods 19 (2013) 216–226.
[12] O. Gsib, et al., Evaluation of fibrin-based interpenetrating polymer networks as potential biomaterials for tissue engineering, Nanomaterials 7 (2017) 436.
[13] A. Shikanov, M. Xu, T.K. Woodruff, L.D. Shea, Interpenetrating fibrin–alginate matrices for in vitro ovarian follicle development, Biomaterials 30 (2009) 5476–5485.
[14] M.A. Salati, et al., Agarose-based biomaterials: opportunities and challenges in cartilage tissue engineering, Polymers (Basel) 12 (2020) 1150.
[15] B.L. Roach, A.B. Nover, G.A. Ateshian, C.T. Hung, Agarose hydrogel characterization for regenerative medicine applications: focus on engineering cartilage, in: Biomaterials From Nature for Advanced Devices And Therapies, John Wiley & Sons, Inc., 2016, pp. 258–273.
[16] M. Alaminos, et al., Construction of a complete rabbit cornea substitute using a fibrin-agarose scaffold, Investig. Opthalmol.Vis. Sci. 47 (2006) 3311.
[17] M. Alaminos, et al., Time-course study of histological and genetic patterns of differentiation in human engineered oral mucosa, J. Tissue Eng. Regen. Med. 1 (2007) 350–359.
[18] V. Carriel, et al., In vitro characterization of a nanostructured fibrin agarose bio-artificial nerve substitute, J. Tissue Eng. Regen. Med. 11 (2017) 1412–1426.
[19] R.K. Das, V. Gocheva, R. Hammink, O.F. Zouani, A.E. Rowan, Stress-stiffening-mediated stem-cell commitment switch in soft responsive hydrogels, Nat. Mater. 15 (2016) 318–325.
[20] A.M.H.P. van den Besselaar, et al., Fibrinogen determination according to Clauss: commutability assessment of international and commercial standards and quality control samples, Clin. Chem. Lab. Med. 55 (2017).
[21] L. Xiang, et al., Combined use of Clauss and prothrombin time-derived methods for determining fibrinogen concentrations: screening for congenital dysfibrinogenemia, J. Clin. Lab. Anal. 32 (2018), e22322.
[22] M. Brunette, et al., Inducible nitric oxide releasing poly-(ethylene glycol)-fibrinogen adhesive hydrogels for tissue regeneration, MRS Proc. 1569 (2013) 39–44.
[23] E. Paramonova, et al., Low-load compression testing: a novel way of measuring biofilm thickness, Appl. Environ. Microbiol. 73 (2007) 7023–7028.
[24] E. Paramonova, O.J. Kalmykowa, H.C. van der Mei, H.J. Busscher, P.K. Sharma, Impact of hydrodynamics on oral biofilm strength, J. Dent. Res. 88 (2009) 922–926.
[25] A. Escudero-Castellanos, B.E. Ocampo-García, M.V. Domínguez-García, J. Flores-Estrada, M.V. Flores-Merino, Hydrogels based on poly(ethylene glycol) as scaffolds for tissue engineering application: biocompatibility assessment and effect of the sterilization process, J. Mater. Sci. Mater. Med. 27 (2016) 176.
[26] S. Nam, J. Lee, D.G. Brownfield, O. Chaudhuri, Viscoplasticity enables mechanical remodeling of matrix by cells, Biophys. J. 111 (2016) 2296–2308.
[27] J.W. Weisel, The mechanical properties of fibrin for basic scientists and clinicians, Biophys. Chem. 112 (2004) 267–276.

[28] A. Montero, et al., Contraction of fibrin-derived matrices and its implications for in vitro human skin bioengineering, J. Biomed. Mater. Res.A 109 (2021) 500–514.
[29] J.W. Weisel, R.I. Litvinov, Fibrin formation, structure and properties, Subcell Biochem. 82 (2017) 405–456.
[30] R. Schapery, Nonlinear viscoelastic solids, Int. J. Solids Struct. 37 (2000) 359–366.
[31] S. Nam, K.H. Hu, M.J. Butte, O. Chaudhuri, Strain-enhanced stress relaxation impacts nonlinear elasticity in collagen gels, Proc. Natl. Acad. Sci. 113 (2016) 5492–5497.
[32] O.A. Ovchinnikova, et al., The collagen cross-linking enzyme lysyl oxidase is associated with the healing of human atherosclerotic lesions, J. Intern. Med. 276 (2014) 525–536.
[33] J.L. Mitchell, N.J. Mutch, Let's cross-link: diverse functions of the promiscuous cellular transglutaminase factor XIII-A, J. Thromb. Haemost. 17 (2019) 19–30.
[34] R.T. Rozenbaum, et al., Role of viscoelasticity in bacterial killing by antimicrobials in differently grown Pseudomonas aeruginosa biofilms, Antimicrob. Agents Chemother. 63 (2019), e01972-18.
[35] I.A. Rodríguez, et al., Rheological characterization of human fibrin and fibrin-agarose oral mucosa substitutes generated by tissue engineering, J. Tissue Eng. Regen. Med. 6 (2012) 636–644.
[36] F.D. Martinez-Garcia, M.M. Valk, P.K. Sharma, J.K. Burgess, M.C. Harmsen, Adipose tissue-derived stromal cells Alter the mechanical stability and viscoelastic properties of gelatine methacryloyl hydrogels, Int. J. Mol. Sci. 22 (2021) 10153.
[37] J.W. Nichol, et al., Cell-laden microengineered gelatin methacrylate hydrogels, Biomaterials 31 (2010) 5536–5544.
[38] G. Solaini, A. Baracca, G. Lenaz, G. Sgarbi, Hypoxia and mitochondrial oxidative metabolism, Biochim. Biophys. ActaBioenerg. 1797 (2010) 1171–1177.
[39] O. Chaudhuri, et al., Hydrogels with tunable stress relaxation regulate stem cell fate and activity, Nat. Mater. 15 (2016) 326–334.
[40] L.T. Vu, G. Jain, B.D. Veres, P. Rajagopalan, Cell migration on planar and three-dimensional matrices: a hydrogel-based perspective, Tissue Eng.B Rev. 21 (2015) 67–74.
[41] C.M. Murphy, M.G. Haugh, F.J. O'Brien, The effect of mean pore size on cell attachment, proliferation and migration in collagen–glycosaminoglycan scaffolds for bone tissue engineering, Biomaterials 31 (2010) 461–466.
[42] K.M. Schultz, K.A. Kyburz, K.S. Anseth, Measuring dynamic cell–material interactions and remodeling during 3D human mesenchymal stem cell migration in hydrogels, Proc. Natl. Acad. Sci. 112 (2015) E3757–E3764.
[43] W.M. Han, Y.C. Jang, A.J. García, The extracellular matrix and cell–biomaterial interactions, in: Biomaterials Science, Elsevier, 2020, pp. 701–715.
[44] C. Pailler-Mattei, S. Bec, H. Zahouani, In vivo measurements of the elastic mechanical properties of human skin by indentation tests, Med. Eng. Phys. 30 (2008) 599–606.
[45] T. Wang, J.H. Lai, F. Yang, Effects of hydrogel stiffness and extracellular compositions on modulating cartilage regeneration by mixed populations of stem cells and chondrocytes in vivo, Tissue Eng.A 22 (2016) 1348–1356.
[46] M. Koch, M.K. Włodarczyk-Biegun, Faithful scanning electron microscopic (SEM) visualization of 3D printed alginate-based scaffolds, Bioprinting 20 (2020), e00098.
[47] A.B. Shrirao, et al., Autofluorescence of blood and its application in biomedical and clinical research, Biotechnol. Bioeng. 118 (2021) 4550–4576.
[48] N.Y. Becerra, et al., Improving fibrin hydrogels' mechanical properties, through addition of silica or chitosan-silica materials, for potential application as wound dressings, Int. J. Biomater. 2021 (2021) 1–11.
[49] R.H.J. de Hilster, et al., Human lung extracellular matrix hydrogels resemble the stiffness and viscoelasticity of native lung tissue, Am. J. Physiol. Cell. Mol. Physiol. 318 (2020) L698–L704.